Available online at www.sciencedirect.com

ScienceDirect

Green Energy & Environment 5 (2020) 433–443

www.keaipublishing.com/gee

Research paper

Enhancing the dynamic electron transfer of Au species on wormhole-like TS-1 for boosting propene epoxidation performance with H_2 and O_2

Dong Lin [a], Xiuhui Zheng [a], Xiang Feng [a,*], Nan Sheng [a], Zhaoning Song [a], Yibin Liu [a], Xiaobo Chen [a], Zhenping Cai [b,*], De Chen [b], Chaohe Yang [a]

[a] *State Key Laboratory of Heavy Oil Processing, China University of Petroleum, Qingdao, 266580, China*
[b] *Department of Chemical Engineering, Norwegian University of Science and Technology, Trondheim, 7491, Norway*

Received 6 July 2020; revised 16 October 2020; accepted 20 October 2020
Available online 21 October 2020

Abstract

Engineering unique electronic structure of catalyst to boost catalytic performance is of prime scientific and industrial importance. Herein, the identification of intrinsic electronic sensitivity for direct propene epoxidation was first achieved over highly stable Au/wormhole-like TS-1 catalyst. Results show that the electron transfer of Au species can be regulated by manipulating the dynamic evolutions and contents of Au valence states, thus resulting in different catalytic performance in 100 h time-on-stream. By DFT calculations, kinetic analysis and multi-characterizations, it is found that the Au^0 species with higher electronic population can easily transfer more electrons to activate surface O_2 compared with Au^{1+} and Au^{3+} species. Moreover, there is a positive correlation between Au^0 content and activity. Based on this correlation, a facile strategy is further proposed to boost Au^0 percentage, resulting in the reported highest PO formation rate without adding promoters. This work harbors tremendous guiding significance to the design of highly efficient Au/Ti-containing catalyst for propene epoxidation with H_2 and O_2.

Keywords: Electron transfer; Valence states; Evolution; Propene epoxidation; DFT

1. Introduction

Propylene oxide (PO) is an essential chemical intermediate which is widely used as the raw material to synthesize polyurethane and polyester resins [1,2]. As an easy operating and eco-friendly process [3–5], direct propene epoxidation with H_2 and O_2 has attracted extensive attention. Since Haruta et al. first found that Au nanoparticles supported on TiO_2 can effectively catalyze this reaction in 1998 [6], different Au/Ti-containing catalysts sprung up like mushrooms [5,7–15]. Based on the well-known reaction mechanism, direct propene epoxidation with H_2 and O_2 requires two active sites including the active Au species and isolated tetrahedral Ti^{4+} sites [13,16], which account for the formation of hydrogen peroxide (H_2O_2) and epoxidation of propene by Ti–OOH intermediate, respectively [9,17–19].

Up to now, considerable attention has been focused on the physico-chemical properties of Au on Ti-containing supports [20,21], such as Au size effect and Au–Ti synergy effect [2,16,22]. However, little attention has been focused on the electronic sensitivity of Au, which was demonstrated to be dominating for precious catalysts, such as Au, Pt, Pd [23–27]. Recently, Yan et al. [28] demonstrated that the metallic Au species are more active than cationic single-atom Au species for CO oxidation reaction. However, Delgass et al. [18] stated that the role of Au species for direct propene epoxidation with H_2 and O_2 should be different from CO oxidation.

* Corresponding authors.
E-mail addresses: xiangfeng@upc.edu.cn (X. Feng), zhenping.cai@ntnu.no (Z. Cai).

https://doi.org/10.1016/j.gee.2020.10.021

Interestingly, Oyama et al. [15] observed that gold (+1) cyanide is selective towards propane by propene hydrogenation. To date, a systematic research on electronic sensitivity of Au for direct propene epoxidation is still lacking. More importantly, there are also no reports on the evolution of Au species at different time-on-stream (e.g., fresh catalysts, pretreated catalysts and used catalysts). Therefore, there is a great need to elucidate the effect of Au electron transfer on catalytic performance, which is highly desirable to design more efficient Au-based catalysts.

To elucidate the electron-dependent performance for direct propene epoxidation, one essential requirement should be fulfilled, i.e., the good stability of the Au/Ti-containing catalysts. This is to ensure the accurate analysis of catalytic performance. Unfortunately, most of Au/Ti-containing catalysts suffer from serious deactivation [3,10]. In our previous work [4], it has been proved that the wormhole-like titanium silicalite-1 (WTS-1) supported Au catalysts can maintain good stability for 100 h without deactivation. As a consecutive effort, Au/WTS-1 catalysts were further employed to investigate the unique electronic sensitivity.

In this work, the electron transfer of Au species was regulated by changing the pretreatment conditions. Under different pretreatments, the dynamic evolution of Au valence states from Au^{1+} to Au^0 and Au^{3+} species during the 100 h catalyst lifetime was different. It is found that there is a positive correlation between catalytic activity and Au^0 content. Combined with multi-characterizations and DFT calculations, it is found that more electrons are transferred from Au^0 to O_2 to activate the adsorbed oxygen species compared with other Au species (Au^{1+} and Au^{3+}), thus boosting the rate-relevant step of PO formation. Moreover, based on this finding, a simple and facile strategy was further established to increase Au^0 content, leading to the reported highest PO formation rate without promoters. This work not only provides a fundamental understanding on the relationship between electron transfer of Au species and catalytic performance, but also harbors tremendous industrial importance to the design of more efficient catalysts for direct propene epoxidation with H_2 and O_2.

2. Experimental Section

2.1. Synthesis of the wormhole-like titanium silicalite-1 (WTS-1)

The WTS-1 was synthesized according to our previous study [4]. In a typical synthesis, 6.90 g of water (H_2O, 18.2 MΩ cm), 27.50 g of tetrapropylammonium hydroxide solution (TPAOH, 25 wt%) and 22.50 g of tetraethyl orthosilicate (TEOS, 98.5 wt%) were mixed and stirred for 2 h. Subsequently, 0.18 g of tetrabutyl titanate (TBOT, 99.0 wt%) dissolved in 20 ml of isopropanol (IPA, 99.7 wt%) was added dropwise. After the evaporation of ethanol at 80 °C for 2 h, the solution was crystallized at 170 °C for 1 day. The as-synthesized TS-1 was washed, dried and calcined at 550 °C. The as-prepared product was seed crystal. Next, 4.00 g of seed crystal, 2.80 g of cetyltrimethyl ammonium bromide (CTAB, 99.0 wt%) and 400 mL of ammonium hydroxide ($NH_3 \cdot H_2O$, 2.5 wt%) were mixed for 3 h. After crystallization at 140 °C for 24 h, the as-obtained product was washed, dried and calcined at 550 °C. The final powder product was denoted as the wormhole-like titanium siliccalite-1 (WTS-1).

2.2. Preparation of the Au/WTS-1 catalysts

The Au/WTS-1 catalysts were synthesized by the improved impregnation method. This method is easy to be scaled up, and could be promising for the future industrialization. The 0.017 g of chloroauric acid ($HAuCl_4 \cdot 4H_2O$, 99.9 wt%) was dissolved in 4.45 g of deionized water (H_2O, 18.2 MΩ cm), then the sodium hydroxide solution (1 mol L^{-1} or 0.1 mol L^{-1}) was added dropwise into the clear yellow solution until the pH of the solution reached 7.3–7.6. After that, 0.5 mL of the solution mentioned above was added to the 0.5 g of WTS-1, and subsequently the wet catalyst was dried overnight at room temperature under vacuum condition. The preparation process was rigidly controlled within 30 min.

2.3. Characterizations

The crystal structure of the WTS-1 was characterized by the X-ray diffraction (XRD, X'pert PRO MPD, Cu K_α radiation). The scanning speed of the X-ray diffraction was 10° min^{-1}. The isolated tetrahedral Ti^{4+} site and anatase (TiO_2) were determined by the ultraviolet-visible spectroscopy (UV-Vis, UV-2700), and the pure $BaSO_4$ was used as the background. The Fourier transform infrared spectroscopy of WTS-1 was recorded on the Fourier-transform spectrometer and the KBr was used as the reference (FT-IR, Nicolet NEXUS 670). The volumetric adsorption analyzer was used to analyze the pore structure of WTS-1 and the degassing temperature was 573 K (Micromeritics 3-Flex 3500). The ^{29}Si MAS NMR spectrum of WTS-1 was recorded on a spectrometer (Varian Unity/Inova, 600 MHz). The size and morphology of the catalyst were observed by the Transmission Electron Microscope (TEM, JEM-2100UHR). The TEM samples were dispersed in alcohol uniformly after ultrasound and were added dropwise onto the ultrathin holey carbon film. In order to restrain the oxidation of Au species, the Au-containing catalysts were under the protection of vacuum before XPS test. The valence states of Au species and active oxygen species were characterized by the X-ray photoelectron spectroscopy (XPS, Escalab 250Xi, Thermo Fisher Scientific, USA) which was performed using a Perkin–Elmer PHI ESCA system, and the C1s binding energy of 284.6 eV was used as the reference. The laser monochromatic Al $K\alpha$ radiation is 18.2 W. The acquisition time is 5.25 min, and the pass energy is 30 eV with a step size of 0.1 eV. The software of XPSPEAK Version 4.0 was used as the XPS peak fitting program.

2.4. Catalytic testing

The catalysts were tested in the gaseous propene epoxidation at 200 °C under atmospheric pressure. 0.15 g of

catalyst (80–100 mesh size) was loaded into a quartz tubular reactor (inner diameter of 8 mm) and the space velocity was 14000 ml $h^{-1}g_{Cat}{}^{-1}$. The reactants include hydrogen (H_2, 3.5 mL min^{-1}, 99.999%), oxygen (O_2, 3.5 mL min^{-1}, 99.999%), propene (C_3H_6, 3.5 mL min^{-1}, 99.999%) and nitrogen (N_2, 24.5 mL min^{-1}, 99.999%). The Au/WTS-1 catalysts were pretreated by three kinds of atmospheres: (1) hydrogen atmosphere, i.e., H_2 (3.5 mL min^{-1}) and N_2 (24.5 mL min^{-1}); (2) oxygen atmosphere, i.e., O_2 (3.5 mL min^{-1}) and N_2 (24.5 mL min^{-1}); (3) feed gas, i.e., H_2 (3.5 mL min^{-1}), O_2 (3.5 mL min^{-1}), C_3H_6 (3.5 mL min^{-1}) and N_2 (24.5 mL min^{-1}). During pretreatment, the catalysts were heated from room temperature to 473 K with the heating rate of 0.5 K min^{-1}. Herein, Au/WTS-1/fresh represents the fresh catalyst before pretreatment; the Au/WTS-1/H-*x*h, O-*x*h and F-*x*h catalysts represent the catalysts pretreated in H_2, O_2 atmosphere and feed gas, respectively. The *x* value of different catalysts represents the reaction time, and 0 h of different catalysts represent the time that pretreatment finishes and reaction initiates.

The products and reactants were analyzed online by gas chromatography (GC, FULI 9790). The TCD and FID detectors were equipped with 5A column and Porapak Q column respectively. The selectivity, conversion and hydrogen efficiency were calculated as follows:

Propene conversion = [(moles of carbon dioxide)/3 + (moles of acetaldehyde × 2)/3 + moles of C_3]/moles of propene;

Hydrogen efficiency = moles of propylene oxide / (moles of H_2 in the feed - moles of H_2 in the product);

Propylene oxide selectivity = moles of propylene oxide / [(moles of carbon dioxide)/3 + (moles of acetaldehyde × 2)/3 + moles of C_3];

Propane selectivity = moles of propane / [(moles of carbon dioxide)/3 + (moles of acetaldehyde × 2)/3 + moles of C_3]

2.5. Density functional theory (DFT) calculation

The DFT calculation was performed by the Vienna ab initio simulation (VASP) using GGA-PBE as the exchange-correlation energy functional. The projected augmented wave potentials were used to explain the interaction between the core and the valence electrons. The plane wave basis was used to expand the Kohn-Sham orbitals and the cutoff energy was 400 eV. In the Brillouin zones, the k-point was set as 4 × 4 × 1 for Au, Au_2O and Au_2O_3 surfaces. The convergence criterion of SCF is 1×10^{-5} eV on energy, and the convergence criterion of geometry optimization is 0.03 eV $Å^{-1}$ for atomic force. In order to be more accurate, two widely used low index facets of Au, Au_2O and Au_2O_3 (e.g. (100) and (111)) were used to adsorb the oxygen, which are the stable surfaces for the Au, Au_2O and Au_2O_3 [29–32]. The surface models were extended to (4 × 4) supercells for Au and (2 × 2) supercells for Au_2O and Au_2O_3. The 10 Å vacuum slab was employed for Au_2O. The 15 Å vacuum slab was used for Au and Au_2O_3 to avoid the pseudo-interactions. All the models were in accordance with stoichiometric ratio of chemical formula. The convergence test of vacuum thickness for the Au_2O surfaces shown in Table S2 and Fig. S17 confirms that the thickness of 10 Å is thick enough to avoid the pseudo-interactions. The fully oxidized models of Au_2O and Au_2O_3 used in the DFT calculation are ideal. The ideal model can guarantee the accurate valence states of Au species (i.e. +1 and + 3) which are in accordance with the experimental results. Therefore, the surface model of different Au species is suitable for the analysis of the O_2 adsorption on the surface of Au species with different valence states. It is also interesting to examine the model of Au valence states regulated by the O atoms at the metal-support interface in the future.

The Bader charge analysis was used to get the atomic charges of Au and O by a fast algorithm. The VESTA visualization software was employed to obtain the charge density differences images, and the computational formula is as follows: $\Delta\rho(r) = \rho_{total}(r) - \rho_{oxygen}(r) - \rho_{support}(r)$, where the $\rho_{total}(r)$, $\rho_{oxygen}(r)$ and $\rho_{support}(r)$ represent the total electron density of the adsorption system, electron densities of oxygen and support, respectively.

3. Results and discussion

3.1. Electron-dependent performance and evolution of Au valence states

Wormhole-like titanium silicalite-1 (WTS-1) was selected as the support for Au deposition. The typical XRD pattern of MFI framework structure (Fig. 1a) is confirmed by the five diffraction peaks at 7.98°, 8.88°, 23.18°, 23.98° and 24.38° [33]. Fig. 1b shows the H4 hysteresis loop in the range of 0.4–0.9, demonstrating the presence of mesopores in the TS-1 [34,35]. The pore size distribution shows two obvious peaks, which are assigned to micropore (0.55 nm) and wormhole-like mesopores (ca. 45 nm). Fig. 1c shows the percentage of surface hydroxyl group, and the peak at −104 ppm is assigned to silicon hydroxyl (i.e., $Si(OSi)_3OH$) [36,37]. Compared with traditional TS-1 support, this WTS-1 sample has less silicon hydroxyls and thus higher hydrophobicity [38,39]. In Fig. 1d, the peak at ca. 210 nm is due to the isolated Ti^{4+} species which are considered as active sites for propene epoxidation. It should be pointed out that there are no peaks at 330 nm, indicating the absence of side phase TiO_2 [20,35]. The FT-IR spectrum is showed in Fig. 1e, and the bands at 550, 800 and 1230 cm^{-1} are usually regarded as the characteristics of TS-1 [40]. The adsorption band at 960 cm^{-1} further confirms the incorporation of Ti into the framework of MFI [41]. Fig. 1f displays the HRTEM image of typical wormhole-like TS-1.

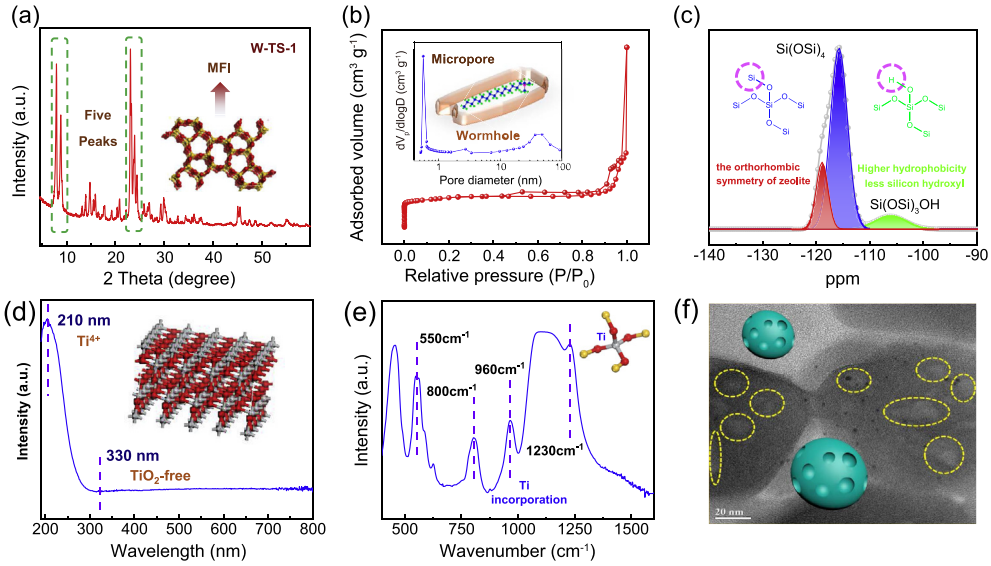

Fig. 1. (a) XRD pattern and (b) Nitrogen adsorption–desorption isotherm of WTS-1, and the inset shows the pore size distribution of WTS-1; (c) ^{29}Si NMR, (d) UV-Vis; (e) FT-IR of WTS-1; (f) typical HRTEM image of Au/WTS-1.

The mesoporous size in the bulk TS-1 is in accordance with the pore size distribution in Fig. 1b.

Three different atmospheres (i.e., H_2, feed gas and O_2) were introduced to tune the electronic properties of Au nanoparticles, and the catalytic performances of three catalysts were shown in Fig. 2. All catalysts can maintain good stability over 100 h due to the high hydrophobicity and low diffusion resistance of WTS-1 [4,10]. The PO formation rate of the three Au/WTS-1 catalysts pretreated in different atmospheres follows the order: H_2 atmosphere > feed gas > O_2 atmosphere. As for PO selectivity, the catalysts after the H_2 pretreatment and feed gas pretreatment are almost the same. However, the selectivity towards PO for the catalyst under O_2 atmosphere is low (only 12%), and the main product is hydrogenated product, i.e., propane (nearly 85%). Fig. S1 shows that the H_2 efficiency of catalysts under different atmospheres follows the following order: feed gas > H_2 atmosphere > O_2 atmosphere. In order to reveal the intrinsic reason for the different performance, the activation energy was first estimated by Arrhenius equation [42], as shown in Fig. 2d–f. All the three activation energies are similar (34.2–38.4 kJ mol^{-1}), which are within the reported range of activation energy for direct propene epoxidation with H_2 and O_2 [43]. This means that the active sites remain the same at different pretreatment atmospheres.

It is well-known that the reaction performance is also strongly affected by the particle size of Au [22,42]. The average Au size of different catalysts was then determined by HRTEM, and more than 100 nanoparticles were counted to guarantee the veracity of particles size. It is found that the size of Au nanoparticles after the H_2 and feed gas pretreatment are similar, but all smaller than that after O_2 pretreatment (Fig. 3). In order to find out whether the poor performance of Au/WTS-1/O catalyst is due to larger Au size, Au/WTS-1/O and Au/WTS-1/F catalysts under O_2 and feed gas pretreatments with similar particle size were further synthesized and compared (Fig. S2 a–d). When the averaged sizes of Au are similar, the PO formation rate of Au/WTS-1/F catalyst is still significantly higher than that of Au/WTS-1/O catalyst. Therefore, the particle size of Au is not the dominating reason for the different catalytic performances. Moreover, it can be clearly seen that the morphology of Au nanoparticles under oxygen pretreatment seems to be spherical shape. However, the morphologies of Au nanoparticles under hydrogen and feed gas pretreatment are truncated cuboctahedron which has the minimum surface free energy for fcc metals [22,44] (Fig. S3). It is reported that truncated cuboctahedral shape can expose more active sites (i.e. corner sites) which can facilitate the adsorption of O_2 molecules and electron transfer from Au nanoparticles to O_2 molecules [22,45–47].

The Au valence states of three catalysts including Au^0, Au^{1+} and Au^{3+} species [48–50] can be determined by XPS. Although the binding energy of Au^0 species could have a shift to influence the location of Au^{1+} species on the reducible TiO_2 support due to the electron transfer between Au^0 species and oxygen vacancies [51], this interaction between Au^0 species and unreducible zeolite can be neglected [52–54]. Fig. 4a shows that the Au^{1+} species were dominant (71%) on the Au/WTS-1/fresh catalyst, which agrees well with the previous results [55,56]. During pretreatments in three kinds of atmospheres, the disproportionated reaction occurs for Au^{1+} species as follows: $3Au^{1+} = 2Au^0 + Au^{3+}$ [57,58]. The detailed compositions of Au species (Table 1) show that the H_2 and feed gas atmosphere can promote the formation of Au^0, while the O_2 atmosphere can restrain the generation of Au^0 species but retain Au^{1+} species on Au/WTS-1. The average valence state shown in Table 1 also shows that the H_2 (0.3) and feed gas (0.41) atmospheres are more beneficial for the generation of Au^0 than O_2 atmosphere (0.85) after propene epoxidation over 100 h. Different percentages of Au species were obtained

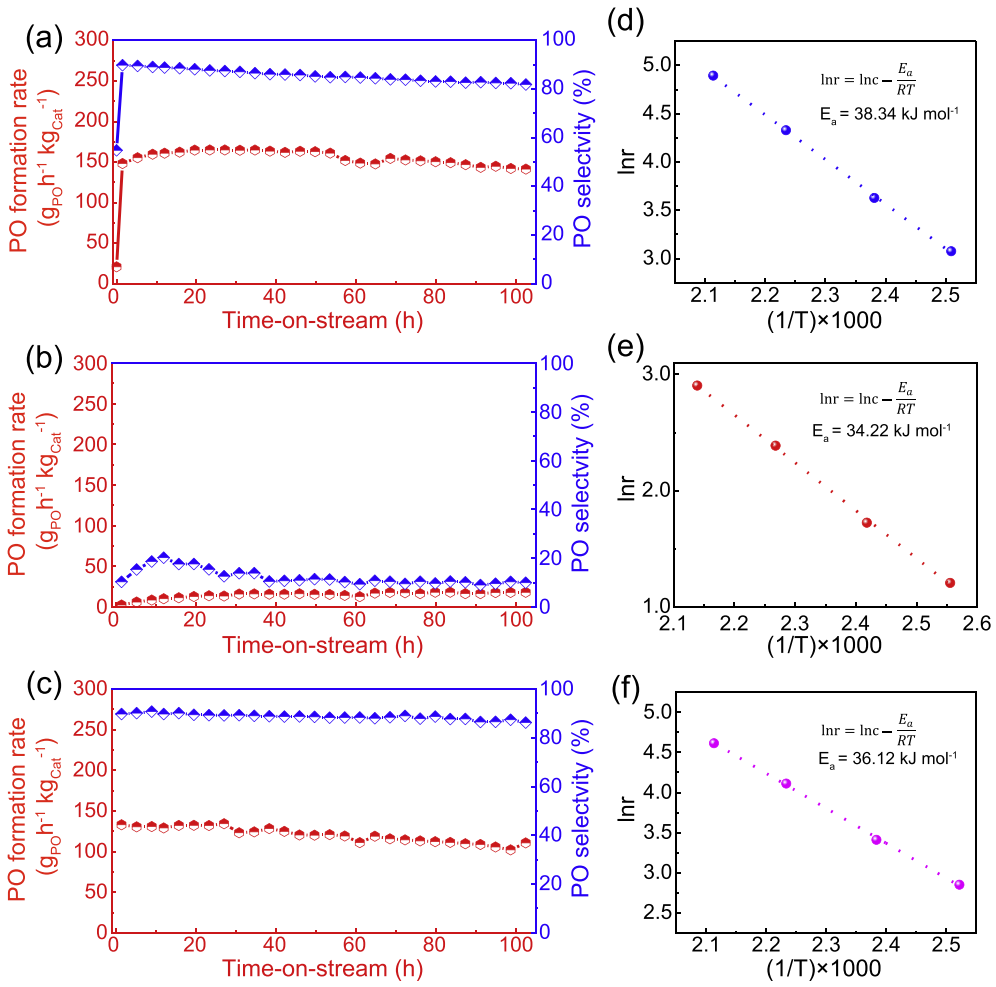

Fig. 2. Reaction performance at 473 K and activation energy of different Au/WTS-1 catalysts under different pretreatment atmospheres: (a,d) H_2, (b,e) O_2, (c,f) feed gas pretreatment.

by varying pretreatment atmospheres. The pretreatment atmospheres can affect the percentage and the evolution of Au valence states, i.e., the disproportionated reaction (from Au^{1+} to Au^{3+} and Au^0) and reduction reaction (from Au^{n+} to Au^0), thus generating different percentages of Au^0.

Different percentages of Au valence states could be affected by the pretreatment atmosphere, morphology of Au nanoparticle and the interaction between metal cluster and support. It is found that the O_2 pretreatment can retain Au^{1+} species and the H_2 or feed gas pretreatments can promote the formation of Au^0 species on the WTS-1. The morphology of Au nanoparticle seems to be spherical shape after O_2 pretreatment while the morphology is typical truncated cuboctahedron after H_2 and feed gas pretreatment. The interaction between Au cluster and support possibly induced by O atoms at the interface may lead to the dynamic evolution of Au valence states, even a chemical looping of valence states.

It should be noted that the Au^0 percentage of the Au/WTS-1/F-0h (84%) is higher than that of the Au/WTS-1/H-0h catalyst (48%), and the initial PO formation rate for Au/WTS-1/F-0h is also higher than that for Au/WTS-1/H-0h. This means that the pretreatment in feed gas is easier to facilitate the formation of Au^0 species than H_2 pretreatment. This should be because propene in feed gas also has reducing ability [59,60].

However, the Au^0 percentage on the Au/WTS-1/F catalyst from 0h to 100 h reaction kept almost unchanged (from 84 to 85%). In contrast, the Au^0 percentage on the Au/WTS-1/H catalyst increased from 48 to 93% in the initial 2 h, and then maintains almost stable (from 93 to 90%) in the rest of 100 h. This confirms that the feed gas after H_2 pretreatment can further promote the reduction of Au^{n+} to Au^0 species. Notably, the change of PO formation rate is closely related to the Au^0 species. The PO formation rate of Au/WTS-1/H catalyst increased from 20 to 141 $g_{PO}h^{-1}$ kg_{Cat}^{-1} in the initial 2 h and also kept stable in the rest of 100 h testing. The stable PO formation rate of Au/WTS-1/H catalyst was better than that of Au/WTS-1/F catalyst. It can also be seen from Fig. 2 that PO selectivity of Au/WTS-1/F and Au/WTS-1/H catalysts all reached ca. 85% for the catalyst, and the dominant Au species on the catalyst are Au^0 species. For Au/WTS-1/O catalyst, the selectivity of propane reached 85%, and the major Au species are Au^{1+} species (85%). The results confirm that the Au^0 species are the active sites for synthesizing PO,

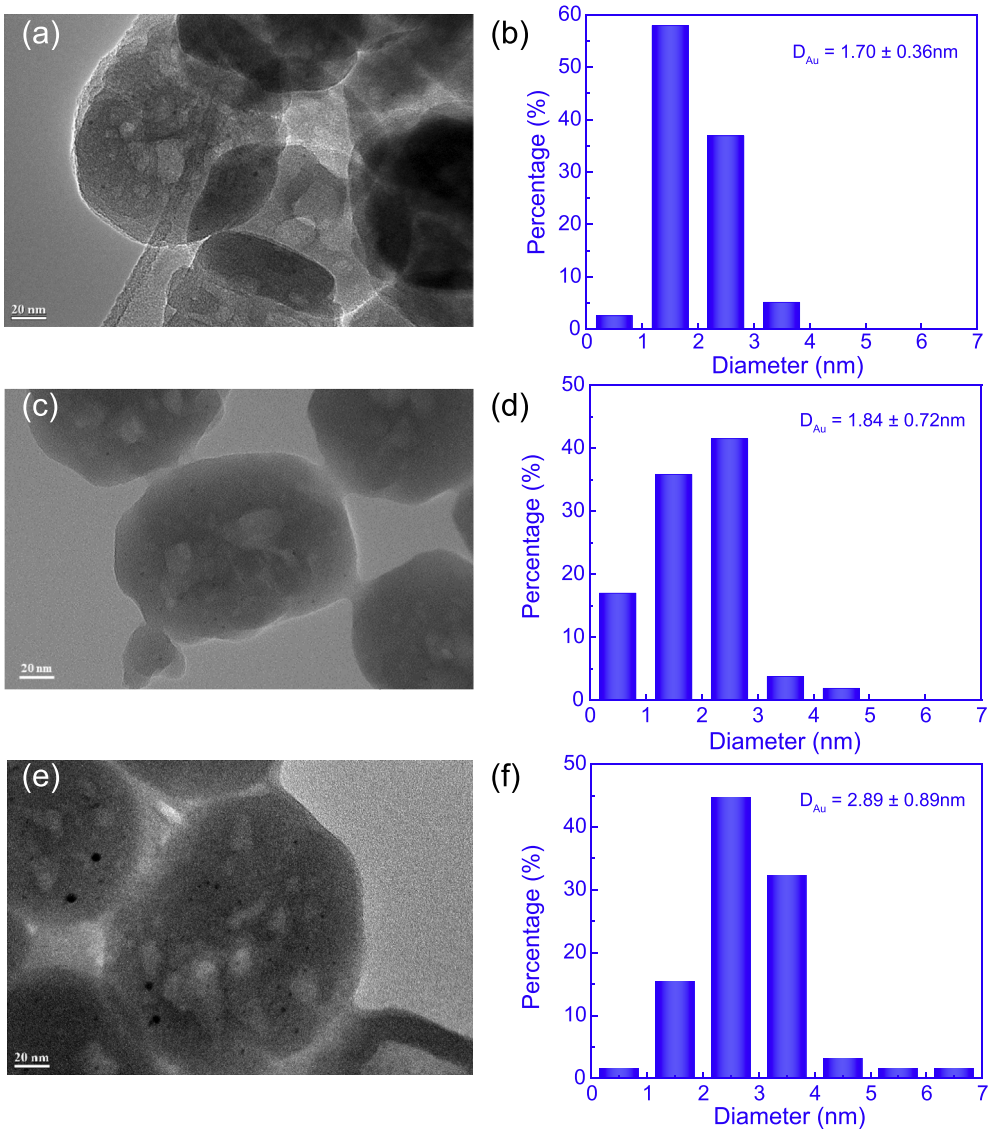

Fig. 3. Representative HRTEM images of Au/W-TS-1 and size distributions of Au nanoparticles under different atmospheres and size distributions of Au nanoparticles: (a–b) hydrogen, (c–d) feed gas, (e–f) oxygen.

and Au^{1+} species are more active towards propane. The converting of the reaction mechanism from propene epoxidation to hydrogenation can be attributed to the valence state of Au species, which is in accordance with Oyama's study [15].

3.2. Intrinsic Au active sites of Au/WTS-1 catalyst

The intrinsic reason for this phenomenon is further studied. According to the well-known reaction mechanism of direct propene epoxidation [9,15,16,61], it is widely accepted that the oxygen becomes surface-active oxygen (O^{2-}) after withdrawing electrons from Au species, and subsequently forms –OOH species. This is the rate-relevant step [2,62]. Therefore, the different Au valence states could affect the number of surface-active oxygen species O^{2-}. The O_{1s} XPS results in Fig. 5 show three kinds of oxygen species on the catalyst, i.e., surface-active O^{2-} species (O_I, 532.5 eV) [9,63,64], oxygen atoms connected with lattice silicon atoms (O_{II}, 533.0 eV) [9,65] and sodium Auger peak and surface hydroxyl groups (O_{III}, 536.5 eV) [66–68]. The surface hydroxyl groups are attributed to the surface silicon hydroxyl (i.e., $Si(OSi)_3OH$). It can be seen that the amount of surface-active O^{2-} species after 100 h testing is the highest on the Au/WTS-1 catalyst under H_2 pretreatment (11.3%) compared with those catalysts under the feed gas (10.9%) and O_2 atmosphere (7.7%). Moreover, the O_2-TPD shown in Fig. S18 also demonstrates that the adsorbing capacity and strength of O_2 follow the order: Au species after H_2 atmosphere pretreatment > feed gas pretreatment > O_2 atmosphere pretreatment, which is consistent with the results of O_{1S} XPS.

DFT calculation was further employed to analyze the effect of atmosphere on the formation of active O^{2-} species. Fig. 6 shows the different adsorption configurations of O_2 on Au, Au_2O and Au_2O_3 systems, which are the calculated relatively

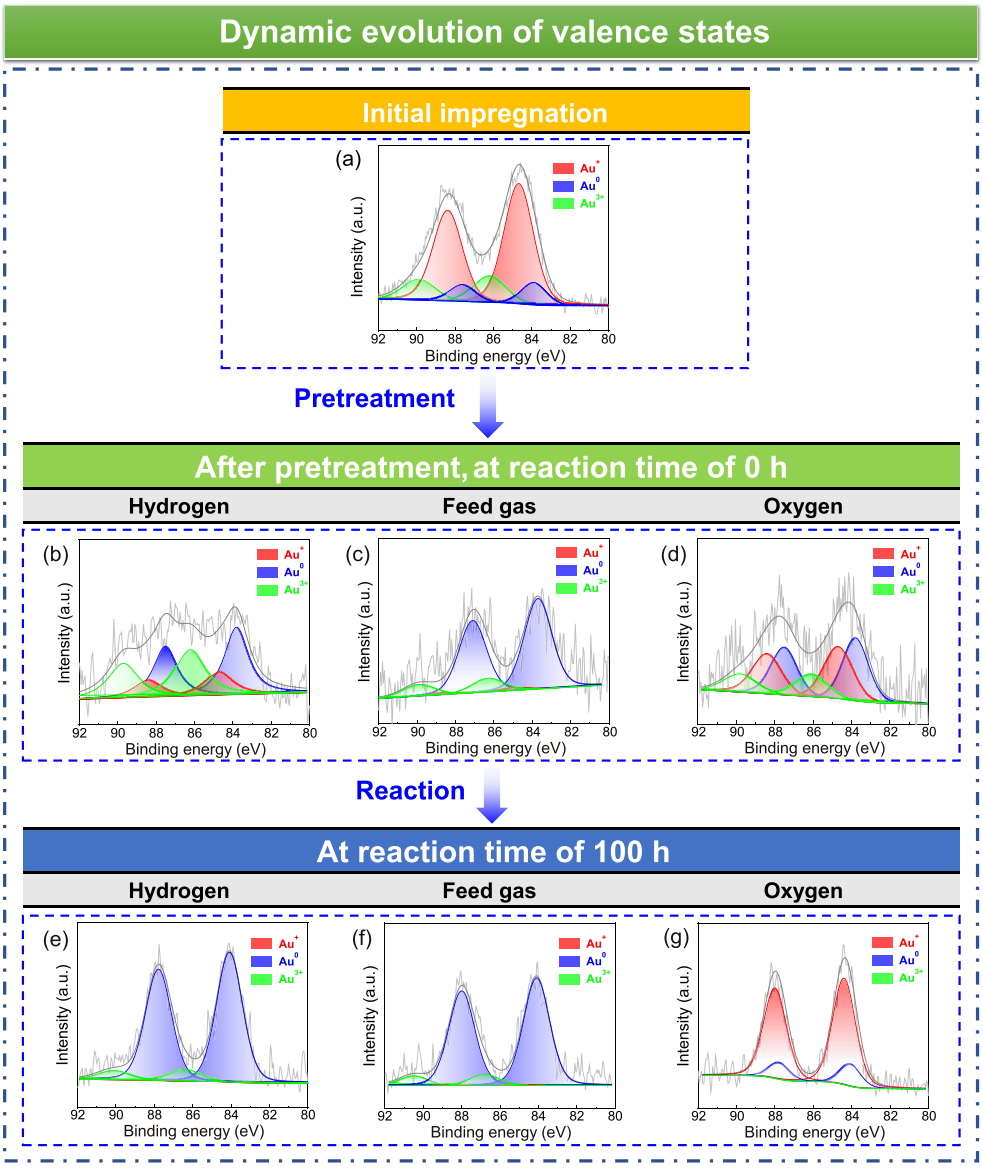

Fig. 4. XPS peaks of Au 4f of various catalysts: (a) the Au/WTS-1 after initial impregnation, (b–g) the Au/WTS-1 pretreated in hydrogen, oxygen and feed gas at different time-on-stream of propene epoxidation (473 K).

stable surface models of different Au species. The rest of the adsorption models were shown in Figs. S4–S15. The bond length of oxygen can be used to judge the activation degree of the O_2 molecule, and the longer length of the O–O bond means a higher degree of activation. It can be clearly seen that the oxygen molecules adsorbed on the Au^0 (100) and (111) surfaces have longer O–O bonds than those on other surfaces of Au_2O and Au_2O_3. Meanwhile, the electronic distribution of

Table 1
Percentages of different Au species on different Au/WTS-1 catalysts in Fig. 4.

Catalyst	Au^0(%)	Au^{1+}(%)	Au^{3+}(%)	Average valence state[j]
(a) Au/WTS-1/fresh	12	71	17	+1.22
(b) Au/WTS-1/H-0h	48	19	33	+1.18
(c) Au/WTS-1/H-100h	90	0	10	+0.30
(d) Au/WTS-1/O-0h	42	39	19	+0.96
(e) Au/WTS-1/O-100h	15	85	0	+0.85
(f) Au/WTS-1/F-0h	84	3	13	+0.42
(g) Au/WTS-1/F-100h	85	2	13	+0.41

(a) Au/WTS-1/fresh represents the catalyst after initial impregnation; (b-g) the Au/WTS-1/H, O and F catalysts represent the catalyst pretreated in hydrogen, oxygen and feed gas at different time-on-stream. (j) The average valence state can be calculated as follows: The average valence state = $0 \times C_0 + 1 \times C_1 + 3 \times C_3$, where C_0, C_1 and C_3 represent the percentage of Au^0, Au^{1+} and Au^{3+}, respectively.

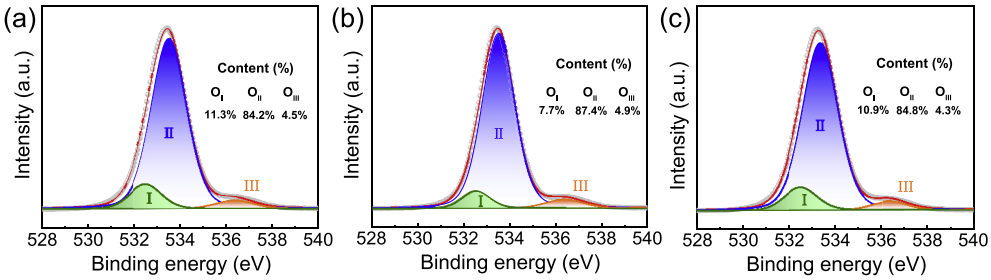

Fig. 5. The XPS spectra of O_{1s} peaks on different catalysts under (a) H_2 atmosphere (b) O_2 atmosphere (c) feed gas after reaction of 100 h.

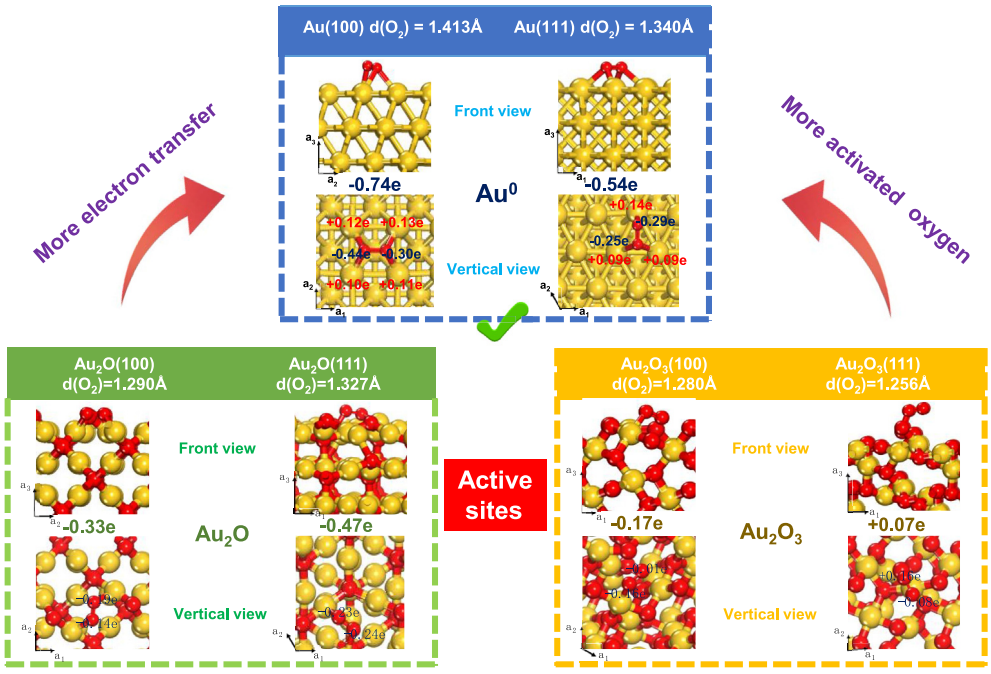

Fig. 6. The electron distributions and bond distances of O_2 molecules absorbed on different surfaces of Au, Au_2O and Au_2O_3.

oxygen was further calculated to elucidate the electron transfer in the Au–O_2 system. It is found that the Au^0 can deliver more electrons (−0.74e and −0.54e) to oxygen molecules than Au^{1+} and Au^{3+} species, which is in accordance with the result of O–O bonds distance. This is mainly because the oxygen molecules withdrawing electrons from Au species are activated by stretching O–O bonds. In addition, the stretching frequency of oxygen was also calculated to measure the degree of activation. According to Table S1, the oxygen molecules absorbed on Au^0 species are close to superoxo forms (O_2^-) and peroxo forms (O_2^{2-}) while the oxygen molecules absorbed on Au^{1+} and Au^{3+} species approach superoxo forms (O_2^-) and oxygen forms (O_2), respectively [69]. The results mean that Au^0 is easier to activate oxygen than Au^{1+} and Au^{3+} species. This is in agreement with the XPS results (Fig. 5).

In order to visualize the electron transfer, the differential charge density was further calculated to show the accumulation or depletion of electrons (Fig. 7). Calamine blue and faint yellow represent the depletion or accumulation of electronic density, respectively. It can be estimated that the oxygen can obtain electrons from Au, Au_2O and Au_2O_3 mostly. Therefore, part of the blue area in the differential charge density plot should be attributed to the electron depletion of the surface. Meanwhile, the $2\pi^*$ antibonding orbital of O_2 obviously gains electrons, while the bonding molecular orbital between two oxygen atoms loses a lot of electrons, so oxygen is activated. Further combined with the results of the Bader charge analysis, we can conclude that Au^0 species can transfer more electrons from surface to oxygen molecules than Au^{1+} and Au^{3+} species, and then more activated oxygen can be used for the subsequent propene epoxidation. Therefore, the more electron transfer and more activated oxygen molecules would be reasons for the higher PO formation rate of Au^0 species.

3.3. A facile strategy to enhance the performance by tuning electron transfer of Au species

Based on our above conclusions, the Au^0 species are active towards the synthesis of propylene oxide (PO) by transferring more electrons to O_2 molecules. Interestingly, there is a positive correlation between the content of Au^0 (in the range of 48–93%) and PO formation rate based on the performance of

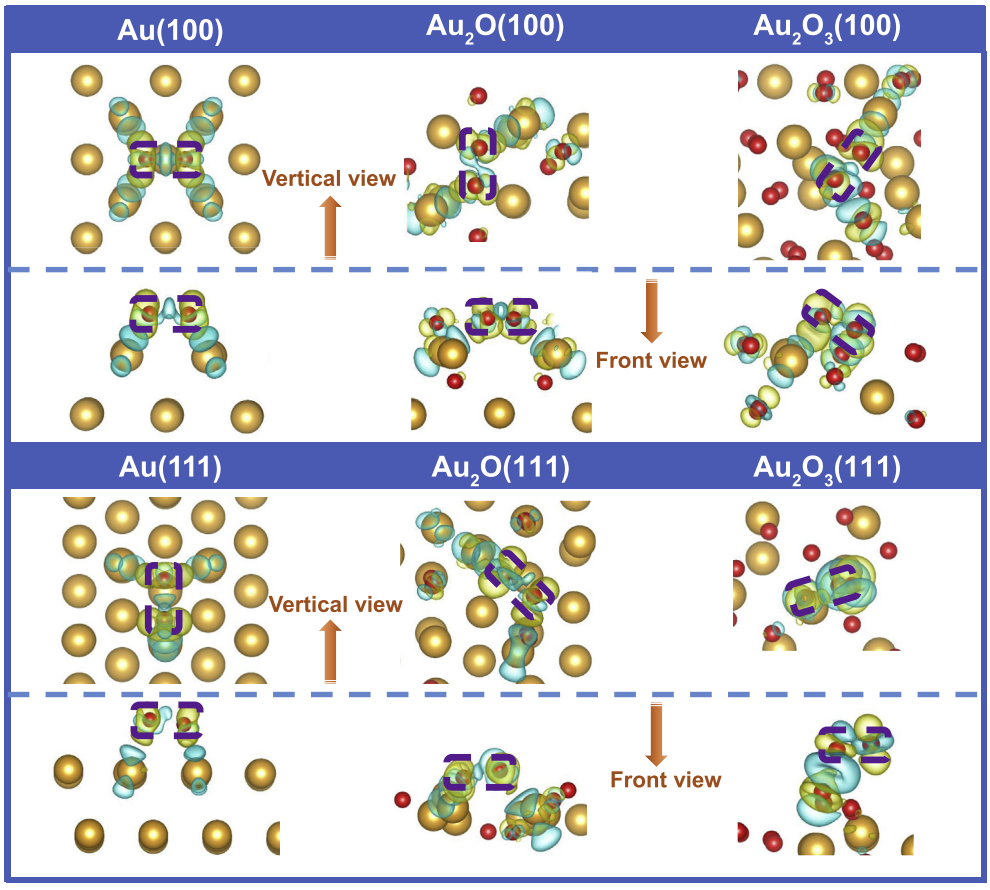

Fig. 7. The differential charge density plots of oxygen molecules adsorbed on various kinds of surfaces of Au, Au_2O and Au_2O_3. Light blue and yellow isosurfaces indicate decrease and increase of 0.005 eV $Å^{-3}$, respectively. The adsorbed oxygen molecule is marked by a purple dotted frame.

different catalysts pretreated in H_2 atmosphere (Fig. 8). This further confirms that Au^0 should be the intrinsic active site. According to this positive correlation, it is expected that the higher PO formation rate may be achieved by increasing the concentration of Au^0 species.

Different pretreatment atmospheres can be used to improve the physicochemical properties of the support and metal nanoparticles in previous studies. Zhou et al. [70] found that the H_2 pretreatment for uncalcined TS-1 can effectively

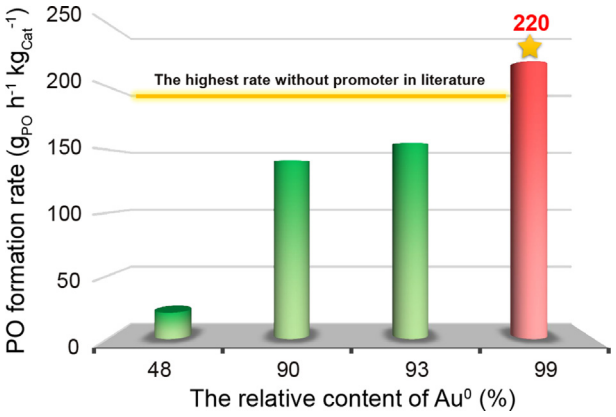

Fig. 8. The positive correlation between PO formation rate and content of Au^0.

increase the binding energy of Ti^{4+} by removing the electron-rich TPA^+ template, thus lowering the electron density and enhancing the PO selectivity. Chen et al. [71] observed that the H_2 pretreatment is in favor of forming smaller metal nanoparticles compared with O_2 pretreatment. Huang et al. [59] demonstrated that H_2 and C_3H_6 dual-component gas pretreatment could cause the formation of small Au nanoparticles and functionalize the surface of TS-1 by hydrophobic hydrocarbon species. The effect of the pretreatment atmosphere mainly focuses on the surface property of support or the steady state of metal nanoparticles, and few researches addressed the dynamic evolution of Au valence state by different pretreatment atmosphere in the life-time catalytic testing. Moreover, since the first report by Haruta [6], the Au/TS-1 catalysts were mostly reduced in feed gas. Herein, a simple and facile strategy was further proposed to enhance the Au^0 percentage. Based on the above results, H_2 pretreatment is effective towards disproportionated reaction, and the following feed gas pretreatment can further reduce Au^{n+}. Therefore, we further prolong the duration of H_2 pretreatment at 200 °C from 400 to 520 min followed by feed gas pretreatment. Fig. 8 shows that the percentage of Au^0 species can reach as high as ca. 99% by this strategy, leading to the highest PO formation rate without promoters (220 $g_{PO}h^{-1}$ $kg_{Cat}{}^{-1}$). Results show that the content of Au species can be regulated by manipulating the dynamic

evolutions and contents of Au valence states, thus resulting in different catalytic performance.

For the first step of propene epoxidation, the absorbed oxygen species on Au (i.e., Au^{1+}, Au^{3+}, Au^{0}) interact with hydrogen to form H_2O_2. The fresh Au/WTS-1 catalyst with abundant Au^{1+} species can be reduced to Au^{0} species by the disproportionated reaction (from Au^{1+} to Au^{3+} and Au^{0}) and reduction reaction (from Au^{n+} to Au^{0}). The Au^{0} species are the intrinsic active sites towards PO formation because they can effectively transfer more electrons to O_2 molecules, generating more O_2^- species. Based on the positive correlation between Au^{0} content and PO formation rate, further increasing content of Au^{0} species can lead to the reported highest PO formation rate without promoter to the best of our knowledge. This result again demonstrates that Au^{0} is the active site towards PO formation. This work shows that the electron transfer of Au species dominates the reaction performance. It harbors significant importance to the design of more efficient Au/Ti-containing catalysts for direct propene epoxidation with H_2 and O_2.

4. Conclusions

In summary, the unique electronic sensitivity of gold was systematically investigated for direct propene epoxidation with H_2 and O_2. Different electronic properties of Au species were achieved by varying pretreatment atmospheres. It can affect the percentage and the evolution of Au valence states, i.e., the disproportionated reaction (from Au^{1+} to Au^{3+} and Au^{0}) and reduction reaction (from Au^{n+} to Au^{0}), thus generating different percentages of Au^{0}. The evolution of Au valence states may be attributed to the O atom at the interface between Au nanoparticle and support. The removal and supplement of O atom at metal-support interface could reduce and increase the Au valence state, respectively, thus further forming chemical looping of valence states. By DFT, kinetic analysis and multi-characterizations, it is found that the Au^{0} with higher electronic population can effectively activate oxygen by stretching the O–O bond, thus donating more electrons to O_2 and forming more active O_2^- species for epoxidation reaction. Based on the positive correlation between the percentages of Au^{0} species and activity, higher Au^{0} percentage can be reached by prolonging H_2 pretreatment followed by feed gas pretreatment. The as-pretreated catalyst shows the reported highest PO formation rate without promoter (~220 $g_{PO}h^{-1}$ kg_{Cat}^{-1}). The results shown in this paper shed new light on the unique electronic sensitivity and the evolution of Au species in direct propene epoxidation with H_2 and O_2. It is of guiding significance to the rational design of efficient Au-containing catalysts.

Conflict of interest

The authors declare that they have no known competing financial interests or personal relationships that could have appeared to influence the work reported in this paper.

Acknowledgments

This work was supported by the Natural Science Foundation of China (21978325, 21776312, 22078364); Key research and development plan of Shandong Province (2019RKE28003, 2018GGX107005); Fundamental Research Funds for the Central Universities (18CX02014A).

Appendix A. Supplementary data

Supplementary data to this article can be found online at https://doi.org/10.1016/j.gee.2020.10.021.

References

[1] J. Huang, T. Takei, T. Akita, H. Ohashi, M. Haruta, Appl. Catal. B Environ. 95 (2010) 430–438.
[2] J.W. Harris, J. Arvay, G. Mitchell, W.N. Delgass, F.H. Ribeiro, J. Catal. 365 (2018) 105–114.
[3] Z. Song, X. Feng, N. Sheng, D. Lin, Y. Li, Y. Liu, X. Chen, D. Chen, X. Zhou, C. Yang, Chem. Eng. J. 377 (2018) 119927.
[4] N. Sheng, Z. Liu, Z. Song, D. Lin, X. Feng, Y. Liu, X. Chen, D. Chen, X. Zhou, C. Yang, Chem. Eng. J. 377 (2018) 119954.
[5] X. Feng, Z. Song, Y. Liu, X. Chen, X. Jin, W. Yan, C. Yang, J. Luo, X. Zhou, D. Chen, ACS Catal. 8 (2018) 10649–10657.
[6] M. Haruta, B. Uphade, S. Tsubota, A. Miyamoto, Res. Chem. Intermediat. 24 (1998) 329–336.
[7] T. Ayvalı, L. Ye, S. Wu, B.T. Lo, C. Huang, B. Yu, G. Cibin, A.I. Kirkland, C. Tang, A.A. Bagabas, J. Catal. 367 (2018) 229–233.
[8] B. Yu, T. Ayvalı, E. Raine, T. Li, M.M.J. Li, J. Zheng, S. Wu, A.A. Bagabas, S.C.E. Tsang, Appl. Catal. B Environ. 243 (2019) 304–312.
[9] X. Feng, J. Yang, X. Duan, Y. Cao, B. Chen, W. Chen, D. Lin, G. Qian, D. Chen, C. Yang, ACS Catal. 8 (2018) 7799–7808.
[10] X. Feng, N. Sheng, Y. Liu, X. Chen, D. Chen, C. Yang, X. Zhou, ACS Catal. 7 (2017) 2668–2675.
[11] Z. Li, W. Ma, Q. Zhong, Ind. Eng. Chem. Res. 58 (2019) 4010–4016.
[12] Z. Li, J. Zhang, D. Wang, W. Ma, Q. Zhong, J. Phys. Chem. C 121 (2017) 25215–25222.
[13] W.S. Lee, M.C. Akatay, E.A. Stach, F.H. Ribeiro, W.N. Delgass, J. Catal. 308 (2013) 98–113.
[14] J. Huang, T. Takei, T. Akita, H. Ohashi, M. Haruta, Appl. Catal. B Environ. 95 (2010) 430–438.
[15] J. Gaudet, K.K. Bando, Z. Song, T. Fujitani, W. Zhang, D.S. Su, S.T. Oyama, J. Catal. 280 (2011) 40–49.
[16] W.S. Lee, L.C. Lai, M.C. Akatay, E.A. Stach, F.H. Ribeiro, W.N. Delgass, J. Catal. 296 (2012) 31–42.
[17] G. Xiong, Y. Cao, Z. Guo, Q. Jia, F. Tian, L. Liu, Phys. Chem. Chem. Phys. 18 (2016) 190–196.
[18] W.S. Lee, R. Zhang, M.C. Akatay, C.D. Baertsch, E.A. Stach, F.H. Ribeiro, W.N. Delgass, ACS Catal. 1 (2011) 1327–1330.
[19] J.J. Bravo-Suárez, K.K. Bando, J. Lu, M. Haruta, T. Fujitani, T. Oyama, J. Phys. Chem. C 112 (2008) 1115–1123.
[20] W.S. Lee, M.C. Akatay, E.A. Stach, F.H. Ribeiro, W.N. Delgass, J. Catal. 287 (2012) 178–189.
[21] X. Feng, X. Duan, G. Qian, X. Zhou, D. Chen, W. Yuan, Appl. Catal. B Environ. 150 (2014) 396–401.
[22] X. Feng, X. Duan, G. Qian, X. Zhou, D. Chen, W. Yuan, J. Catal. 317 (2014) 99–104.
[23] Y.Z. Chen, Z.U. Wang, H. Wang, J. Lu, S.H. Yu, H.L. Jiang, J. Am. Chem. Soc. 139 (2017) 2035–2044.
[24] C. Cui, L. Gan, M. Heggen, S. Rudi, P. Strasser, Nat. Mater. 12 (2013) 765–771.

[25] M. Guo, H. Li, Y. Ren, X. Ren, Q. Yang, C. Li, ACS Catal. 8 (2018) 6476–6485.
[26] Y. Lou, J. Ma, W. Hu, Q. Dai, L. Wang, W. Zhan, Y. Guo, X.M. Cao, Y. Guo, P. Hu, ACS Catal. 6 (2016) 8127–8139.
[27] W.E. Kaden, T. Wu, W.A. Kunkel, S.L. Anderson, Science 326 (2009) 826–829.
[28] L.W. Guo, P.P. Du, X.P. Fu, C. Ma, J. Zeng, R. Si, Y.Y. Huang, C.J. Jia, Y.W. Zhang, C.H. Yan, Nat. Commun. 7 (2016) 13481.
[29] R.P. Ren, L. Cheng, Y.K. Lv, Surf. Sci. 630 (2014) 116–124.
[30] S. Klaus, L. Trotochaud, M.J. Cheng, M. Head-Gordon, A.T. Bell, ChemElectroChem 3 (2016) 66–73.
[31] M. Liu, M. Liu, X. Wang, S.M. Kozlov, Z. Cao, P. De Luna, H. Li, X. Qiu, K. Liu, J. Hu, C. Jia, P. Wang, H. Zhou, J. He, Z. Miao, X. Lan, Y. Zhou, Z. Wang, J. Li, A. Seifitokaldani, C. Thang Dinh, H. Liang, C. Zou, D. Zhang, Y. Yang, T. Chan, Y. Han, L. Cavallo, T. Sham, B. Hwang, E.H. Sargent, Joule 3 (2019) 1703−1718.
[32] X. Yu, X. Zhang, X. Tian, S. Wang, G. Feng, Appl. Surf. Sci. 324 (2015) 53–60.
[33] R. Khomane, B. Kulkarni, A. Paraskar, S. Sainkar, Mater. Chem. Phys. 76 (2002) 99–103.
[34] S. Mintova, M. Hölzl, V. Valtchev, B. Mihailova, Y. Bouizi, T. Bein, Chem. Mater. 16 (2004) 5452−5459.
[35] Z. Wang, L. Xu, J.G. Jiang, Y. Liu, M. He, P. Wu, Micropor. Mesopor. Mat. 156 (2012) 106–114.
[36] H. Wang, T.J. Pinnavaia, Angew. Chem. Int. Edit. 45 (2006) 7603−7606.
[37] Z. Wu, S. Goel, M. Choi, E. Iglesia, J. Catal. 311 (2014) 458–468.
[38] X. Feng, D. Chen, X. Zhou, RSC Adv. 6 (2016) 44050–44056.
[39] S. Du, X. Chen, Q. Sun, N. Wang, M. Jia, V. Valtchev, J. Yu, Chem. Commun. 52 (2016) 3580−3583.
[40] L. Xu, Y. Ren, H. Wu, Y. Liu, Z. Wang, Y. Zhang, J. Xu, H. Peng, P. Wu, J. Mater. Chem. 21 (2011) 10852−10858.
[41] D. Serrano, R. Sanz, P. Pizarro, I. Moreno, S. Medina, Appl. Catal. B Environ. 146 (2014) 35–42.
[42] W. Chen, J. Ji, X. Feng, X. Duan, G. Qian, P. Li, X. Zhou, D. Chen, W. Yuan, J. Am. Chem. Soc. 136 (2014) 16736−16739.
[43] W.-S. Lee, M.C. Akatay, E.A. Stach, F.H. Ribeiro, W.N. Delgass, J. Catal. 313 (2014) 104−112.
[44] Q. Zhu, M. Liang, W. Yan, W. Ma, Micropor. Mesopor. Mat. 278 (2019) 307−313.
[45] S. Karra, M. Wooten, W. Griffith, W. Gorski, Electrochim. Acta 218 (2016) 8−14.
[46] H. Wang, C. Chen, Y. Zhang, L. Peng, S. Ma, T. Yang, H. Guo, Z. Zhang, D.S. Su, J.J.N.c. Zhang, Nat. Commun. 6 (2015) 1−6.
[47] L. Hu, Q. Peng, Y.J. Li, J. Am. Chem. Soc. 130 (2008) 16136−16137.
[48] K. Zhou, W. Wang, Z. Zhao, G. Luo, J.T. Miller, M.S. Wong, F. Wei, ACS Catal. 4 (2014) 3112−3116.
[49] X. Liu, M. Conte, D. Elias, L. Lu, D.J. Morgan, S.J. Freakley, P. Johnston, C.J. Kiely, G.J. Hutchings, Catal. Sci. Technol. 6 (2016) 5144−5153.
[50] Z. Huo, C.K. Tsung, W. Huang, X. Zhang, P. Yang, Nano Lett. 8 (2008) 2041−2044.
[51] J. Radnik, C. Mohr, P. Claus, Phys. Chem. Chem. Phys. 5 (2003) 172−177.
[52] J. Lee, S.P. Burt, C.A. Carrero, A.C. Alba-Rubio, I. Ro, B.J. O'Neill, H.J. Kim, D.H. Jackson, T.F. Kuech, I.J.J.o.C. Hermans, J. Catal. 330 (2015) 19–27.
[53] D. Liu, Y.Q. Xian, N.E.C. Wei, R. Lau, A. Borgna, Y.J. Yang, J. Catal. 266 (2009) 380–390.
[54] L. Wang, L. Wang, X. Meng, F.S. Xiao, Adv. Mater. 31 (2019) 1901905.
[55] M.V. Kirichkov, A.A. Guda, A.P. Budnyk, A.L. Bugaev, T.A. Lastovina, V.V. Shapovalov, S.A. Guda, A.L. Trigub, Y.V. Rusalev, A.V. Chernyshev, Radiat. Phys. Chem. (2018) (2020) 108067.
[56] S.Y. Chang, A. Uehara, S.G. Booth, K. Ignatyev, J.F.W. Mosselmans, R.A. Dryfe, S.L. Schroeder, RSC Adv. 5 (2015) 6912–6918.
[57] C. Li, F. Fan, B. Yin, L. Chen, T. Ganguly, Z. Tian, Nano Res. 6 (2013) 29–37.
[58] R. Küster, K. Seppelt, Z. Anorg. Allg. Chem. 626 (2000) 236–240.
[59] Y.G. Ren, J. Huang, Q. Lv, Y. Xie, A.H. Lu, M. Haruta, Appl. Catal. Gen. 584 (2019) 117172.
[60] J. Lu, J.J. Bravo-Suárez, A. Takahashi, M. Haruta, S.T. Oyama, J. Catal. 232 (2005) 85–95.
[61] A. Sinha, S. Seelan, S. Tsubota, M. Haruta, Top. Catal. 29 (2004) 95−102.
[62] E.E. Stangland, K.B. Stavens, R.P. Andres, W.N. Delgass, J. Catal. 191 (2000) 332−347.
[63] J.H. Zhou, Z.J. Sui, J. Zhu, P. Li, D. Chen, Y.C. Dai, W.K. Yuan, Carbon 45 (2007) 785−796.
[64] Y. Wei, Z. Zhao, J. Liu, S. Liu, C. Xu, A. Duan, G. Jiang, J. Catal. 317 (2014) 62–74.
[65] H. Liu, G. Lu, H.J.M.c. Hu, physics, Mater. Chem. Phys. 100 (2006) 162−167.
[66] Q. Li, Y. Zhang, G. Chen, J. Fan, H. Lan, Y.J.J.o.C. Yang, J. Catal. 273 (2010) 167−176.
[67] R. Thangavel, A.G. Kannan, R. Ponraj, X. Sun, D.W. Kim, Y.S. Lee, J. Mater. Chem. 6 (2018) 9846−9853.
[68] D. Luo, J. Xu, Q. Guo, L. Fang, X. Zhu, Q. Xia, H.J.A.F.M. Xia, Adv. Funct. Mater. 28 (2018) 1805371.
[69] R. Zhang, H. Liu, H. Zheng, L. Ling, Z. Li, B. Wang, Appl. Surf. Sci. 257 (2011) 4787−4794.
[70] G. Wang, Y. Cao, Z. Zhang, J. Xu, M. Lu, G. Qian, X. Duan, W. Yuan, X. Zhou, Ind. Eng. Chem. Res. 58 (2019) 17300−17307.
[71] L. Yang, Y. Kimmel, Q. Lu, J. Chen, J. Power Sources 287 (2015) 196–202.